ORIGINAL ARTICLE

Characterization of the surface morphology and grain growth near the surface of a block copolymer thin film with cylindrical microdomains oriented perpendicular to the surface

Shinichi Sakurai[1], Toshimasa Harada[1], Hiroshi Ohnogi[1], Toshiyuki Isshiki[2] and Sono Sasaki[1]

A surface morphology characterization was conducted via atomic force microscope (AFM) observations using thin film specimens of a polystyrene-*block*-poly(ethylene-*co*-butylene)-*block*-polystyrene triblock copolymer with perpendicularly oriented polystyrene cylinders. We sought to determine whether the cylinders were oriented parallel or perpendicular to the film specimen at the near-surface region. Furthermore, the grain size was successfully evaluated using the AFM observations with an image analysis method using Fourier transform (FT)/inverse FT techniques for the grains at the near-surface region of the thin film specimen. The grain size in the interior of the specimen was also evaluated using small-angle X-ray scattering measurements. From the comparison of the results, it was found that the grains were slightly larger (~53% larger) on the surface than in the interior of the specimen. However, this difference might have been due to differences in the evaluation methods. Nevertheless, both results for the grain growth on the surface and in the interior of the specimen exhibited power-law behavior with the same exponent (~0.45) with < 55 min of thermal annealing, in which the cylinders gradually oriented perpendicular to the film surface while simultaneously improving the hexagonal lattice regularity. By contrast, with more than 55 min of thermal annealing, an abrupt increase in the grain size was noticeable both on the surface and in the interior of the sample. Therefore, it can be concluded that the grains could not grow quickly during the structural changes in the interior of the specimen (progressive perpendicular orientation of the cylinders and improvement in the hexagonal lattice regularity). After completing the orientation and achieving lattice regularity, the grains were finally able to grow quickly.
Polymer Journal (2017) **49**, 655–663; doi:10.1038/pj.2017.36; published online 2 August 2017

INTRODUCTION

Block copolymers have been widely utilized in a variety of applications as thermoplastic elastomers, nanotemplates, adhesives and so forth. Recently, intensive efforts have focused on controlling the mechanical and optical properties of thin-layered block copolymer films for the purpose of using the block copolymer materials as adhesives, coating films, packaging films and so on. As those properties are closely related to the microdomain structures (the morphology and orientation of the microdomains), their characterization is very important. Furthermore, the contribution of the surface structure to the macroscopic properties of the block copolymer thin film becomes increasingly significant when its thickness decreases. To characterize the nanostructures on free surfaces, atomic force microscope (AFM) observations have generally been conducted;[1–6] computer simulations are also a powerful tool,[2,7] and grazing-incidence small-angle X-ray scattering[8–14] measurements have become a recent trend in block copolymer thin film studies. Very recently, we have utilized the conventional method of transmission-mode small-angle X-ray scattering (SAXS) with a material that was 'transparent' to X-rays as a substrate, on which a block copolymer film was cast or spin-coated.[15,16] In the current study, this conventional transmission-mode SAXS method was utilized to analyze the morphology and orientation of cylinders on the surface of a block copolymer thin film. The result of a computer simulation implies that the orientational state is different in the outermost layer of the block copolymer specimen compared to the orientation in the interior of the specimen. Thus, we sought to check this conclusion by conducting AFM observations to determine whether the cylinder orientation is parallel or perpendicular to the film specimen with perpendicularly oriented cylinders. Furthermore, we evaluated the grain size of the cylindrical microdomains in the proximity of the surface by applying a simple image analysis method that has been reported recently.[17] On the basis of these results, the grain growth will be discussed and compared with that for the grains existing in the interior of the specimen.

The term 'grain' refers to a higher-ranking hierarchical structure of block copolymer microdomains.[18] Even for the case of cylinders that are uniformly oriented, different grains can be identified, as schematically illustrated in Figure 1. Here a polygrain state is illustrated for

[1]Department of Biobased Materials Science, Kyoto Institute of Technology, Matsugasaki, Sakyo-ku, Kyoto, Japan and [2]Faculty of Electrical Engineering and Electronics, Kyoto Institute of Technology, Matsugasaki, Sakyo-ku, Kyoto, Japan
Correspondence: Professor S Sakurai, Department of Biobased Materials Science, Kyoto Institute of Technology, Matsugasaki, Sakyo-ku, Kyoto 606-8585, Japan.
E-mail: shin@kit.ac.jp

656

the cylinders oriented perpendicular to the surface. Note that the white arrows exhibit the orientational direction of the hexagonal lattice (one of the three $\langle 10\bar{1}0 \rangle$ directions). We can evaluate the average size of such grains near the surface using image analysis[17] with the AFM results and in the interior of the specimen using SAXS.[18]

EXPERIMENTAL PROCEDURES

The sample used in this study was a polystyrene-*block*-ploy(ethylene-*co*-butylene)-*block*-polystyrene (SEBS) triblock copolymer with $M_n = 6.60 \times 10^4$ and $M_w/M_n = 1.03$ (M_n: number-average molecular weight; M_w: weight-average molecular weight). The total volume fraction of the polystyrene (PS) end blocks was 0.16. As the middle poly(ethylene-*co*-butylene) (PEB) block comprised ethylene and butylene moieties, the composition was clarified as having an ethylene/butylene ratio of 59/41 (by volume). Therefore, the overall composition in the SEBS sample was (PS end block)/(ethylene moiety in PEB)/(butylene moiety in PEB)/(PS end block) equal to 8/50/34/8.

Thin films of the triblock copolymer with a thickness in the range of 45–175 μm were prepared on polyimide tape (Nitto Denko Co., Ltd., Osaka, Japan) using the solution-casting method. The scheme of film preparation is schematically shown in Figure 2. First, the polyimide tape was attached onto a Si wafer (Yamanaka Hutech Co., Kyoto, Japan). Then, the surface of the polyimide tape was carefully contacted on the surface of the polymer solution. Owing to the surface tension, a small amount of the polymer solution was transferred onto the surface of the polyimide tape. Then, the substrate was flipped over to bring the small amount of the transferred solution face up. After complete solvent evaporation, a dried thin film developed on the polyimide tape. Subsequently, they were placed in a high-temperature oven, purged with N_2 gas, thermally annealed under a N_2 atmosphere at 210 °C for various durations (10–60 min) and immediately quenched in ice water. These specimens were subjected to AFM observations and SAXS measurements at room temperature. Note here that the AFM observations were conducted using specimens on polyimide tape attached to Si wafers, while the SAXS measurements were performed using specimens on polyimide tape detached from Si wafers because the Si wafer blocked the incident X-ray beam, disabling the transmission-mode SAXS measurements.

A selective solvent, *n*-heptane, was used for the solution casting because *n*-heptane is a good solvent for PEB and a poor solvent for PS. To enhance the solubility, methylene chloride, which is an inversely selective solvent (good for PS while very poor for PEB), was used as a cosolvent, such that a 1:1 mixture of *n*-heptane/methylene chloride was actually used. As methylene chloride is volatile at room temperature, it evaporated rapidly from the 5% solution of the SEBS sample. After the methylene chloride completely evaporated, the *n*-heptane still remained in the solution and the *n*-heptane solution of the SEBS sample was finally obtained. Subsequently, the remaining *n*-heptane completely evaporated for several days at room temperature, and the as-cast specimen was obtained.

To evaluate the grain size on the surface of the specimens annealed at 210 °C for various durations, the AFM observations were conducted using an SPM-9600 (SHIMADZU, Kyoto, Japan) and a cantilever of PPP-SEIHR-20 (NANO*SENSORS*, Neuchatel, Switzerland) with a length of 225 μm, force constant of 5–37 N m^{-1} and resonance frequency of 130 kHz.

The specimen for the SAXS measurement was cut and peeled from the Si wafer that was used for the AFM observation. The SAXS measurements were carried out, using the peeled polyimide tape on which the thin layer of the specimen was placed (the adhesive on the polyimide tape was carefully removed by wiping with toluene before the SAXS measurement), at the BL-10C beamline of the Photon Factory, High Energy Accelerator Research Organization, Tsukuba, Japan,[19] using X-rays with a wavelength of 0.1488 nm. This beamline provides a quasi point-focused beam by using a toroidal mirror, and the beam size was measured at the detector position, which was 850 μm in the vertical direction and 1000 μm in the horizontal direction. A standard slit system with widths of 0.7×0.7 mm was used for the SAXS collimation. At this condition, the brightness of the X-ray beam was 4.1×10^9 phs s^{-1}. A PILATUS300K–W (Dectris, Baden, Switzerland), which has three pieces of rectangular-shaped X-ray-sensitive elements (83.8×33.5 mm in size and 487×195 pixels with 172 μm pixel size) that are arranged in a series so that the long edges of the elements are in line with each other (in total, the actual size was 254×33.5 mm), was used with its long axis parallel to the vertical direction. The sample-to-detector distance was 2040 mm. Along the long edge of the detector, the sensitive *q*-range was -2.62 nm$^{-1} < q < 2.62$ nm^{-1} (because of the symmetrical arrangement of the detector), and along the short edge of the detector, the sensitive *q*-range was -0.35 nm$^{-1} < q < 0.35$ nm^{-1}. Here *q* denotes the magnitude of the scattering vector, defined as follows:

$$q = \frac{4\pi}{\lambda} \sin \frac{\theta}{2} \qquad (1)$$

where λ and θ are the X-ray wavelength and the scattering angle, respectively. The two-dimensional SAXS (2d-SAXS) patterns were further converted to one-dimensional profiles by sector averaging in the range $\phi \pm 2.5°$ of the azimuthal angle, where ϕ denotes the azimuthal angle for the direction of the reflection peak appearing.

RESULTS AND DISCUSSION

Figure 3a shows the AFM image (phase image) of the as-cast SEBS specimen, while Figure 3b–h show those of the annealed
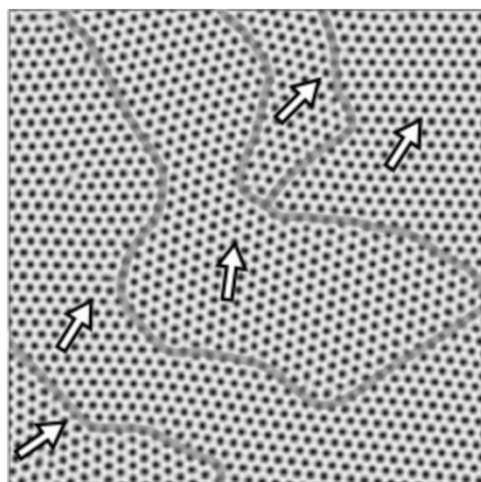

Figure 1 Schematic illustration of the polygrain state in the material in which the cylindrical axes are oriented perpendicularly. Note that the white arrows exhibit the orientation direction of the hexagonal lattice (one of the three $\langle 10\bar{1}0 \rangle$ directions).
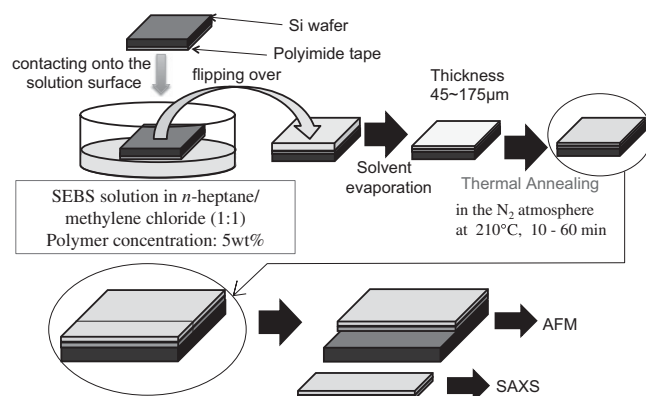

Figure 2 Schematic illustration showing the preparation method of the thin film specimens for atomic force microscope (AFM) observations and small-angle X-ray scattering (SAXS) measurements. Note here that the polyimide tape with a thickness of 25 μm is transparent to the X-rays. A full color version of this figure is available at *Polymer Journal* online.
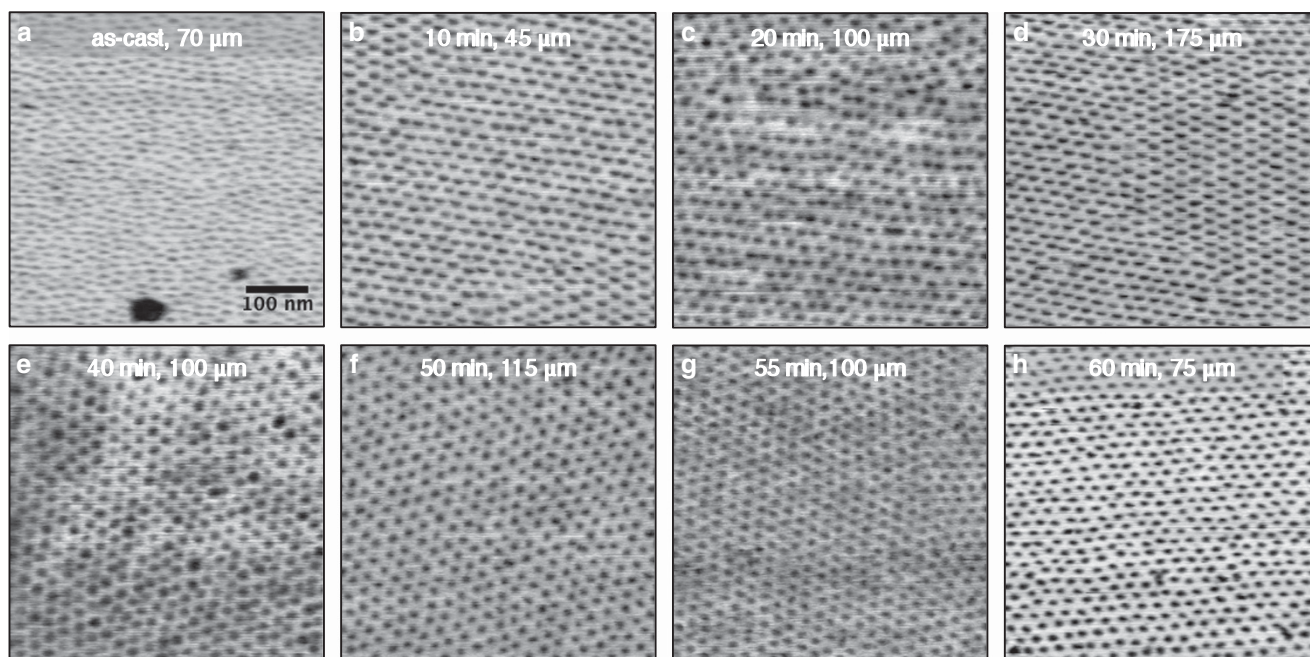
Figure 3 (**a**) Atomic force microscope image (phase image) of the as-cast SEBS specimen and (**b–h**) those of the annealed SEBS specimens in which cylindrical microdomains are perpendicularly oriented to the film. The annealing was conducted at 210 °C for various durations, as indicated in the figure.

SEBS specimens in which the cylindrical microdomains were perpendicularly oriented to the surface of the film specimen. The annealing was conducted at 210 °C under a nitrogen atmosphere for various durations indicated in the figure. Figure 4 shows the corresponding Fourier transform (FT) patterns obtained for the images shown in Figure 3 using the free ImageJ software program.[20] The scale bar indicated in Figure 4a is defined as $2\pi/d$, where d denotes spacing in the real space image.

For the as-cast specimen, dark elliptic particles can be seen in Figure 3a. As the darker part in this phase image corresponds to the harder part, these particles can be recognized as PS microdomains. As the FT image for this specimen shows a single donut-shaped elliptic ring, the packing regularity is found to be poor. It is already known that these particles are non-equilibrium PS spherical microdomains[21,22] that are kinetically locked in the as-cast specimen due to the PS vitrification. The non-equilibrium PS spherical microdomains are considered to be formed in the solution at a specific concentration as the effective volume fraction of PS in the *n*-heptane solution was shifted to a lower value because of the selective solubility of the PEB chains in *n*-heptane. After the *n*-heptane evaporated completely, the non-equilibrium PS spheres vitrified in the as-cast film. As reported in our previous study,[21,22] the spheres transformed into cylinders with their long axes perpendicular to the specimen surface by thermally annealing the as-cast film at a temperature (210 °C) sufficiently higher than the T_g of PS (55.9 °C).[23] Not only for the perpendicular orientation but also for the parallel orientation of the cylinders, such kinetically locked non-equilibrium spheres can possibly be used to control the orientation through directional coalescence with an external field. As a matter of fact, excellent parallel cylinder orientation has been attained by the application of planar flow on as-cast specimens at high temperatures ($> T_g$).[24,25] By contrast, preferential orientation has not been observed when uniaxially stretched as-cast specimens were thermally annealed at high temperature ($> T_g$); the stretched specimens were sandwiched

between two pieces of slide glass to prevent the immediate breakdown of the stretched specimen upon thermal annealing.[6]

It was reported in our previous publication that such kinetically locked non-equilibrium spheres become slightly deformed, as detected using a transmission electron microscope in the interior of the specimen.[22] Thus, a similar tendency is seen on the surface in Figure 3a as well. As the spherical microdomains are unstable, they may deform into elongated shapes in the course of or even after the vitrification of the PS phase during the solvent evaporation. This phenomenon led to the observation of elongated spheres on the surface of the as-cast specimen as shown in Figure 3a. Contrary to Figure 3a, the images show nearly round-shaped microdomains in Figure 3b–h. Furthermore, the packing regularity is found to be higher because the spotty FT patterns are found in Figure 4b–h. As stated below, the SAXS results definitely indicate that PS cylinders were formed in those specimens. Therefore, the AFM results imply that the PS cylinders were also oriented perpendicular to the film surface. Note here that the AFM images shown in Figure 3 may mislead readers into considering that the PS cylinders protruded outward at the surface. However, the surface should have been covered with the component bearing the lower surface free energy. As the surface free energy for PS is 40.2 mJ m^{-2} and that for PEB is 23 mJ m^{-2},[26] PEB should have covered the surface. To meet this requirement, a structure model is proposed on the basis of the results of the AFM height image in Figure 5a. From the AFM height image, the topological profile was extracted along the A–B line. The PS cylinder diameter of 10.8 nm, the intercylinder distance of 25.5 nm and the hump of 3.5 nm on the surface were found in the A–B topological profile. Although the volume fraction of PS evaluated from these numerical values is 0.16, which is identical to the volume fraction of the PS in the SEBS triblock copolymer, the cylinder near the surface is found to be smaller (86%) than that in the interior of the specimen. The thickness of the outermost PEB layer can be estimated by assuming a core-shell hemisphere near the surface (as shown in Figure 5b). Then, the
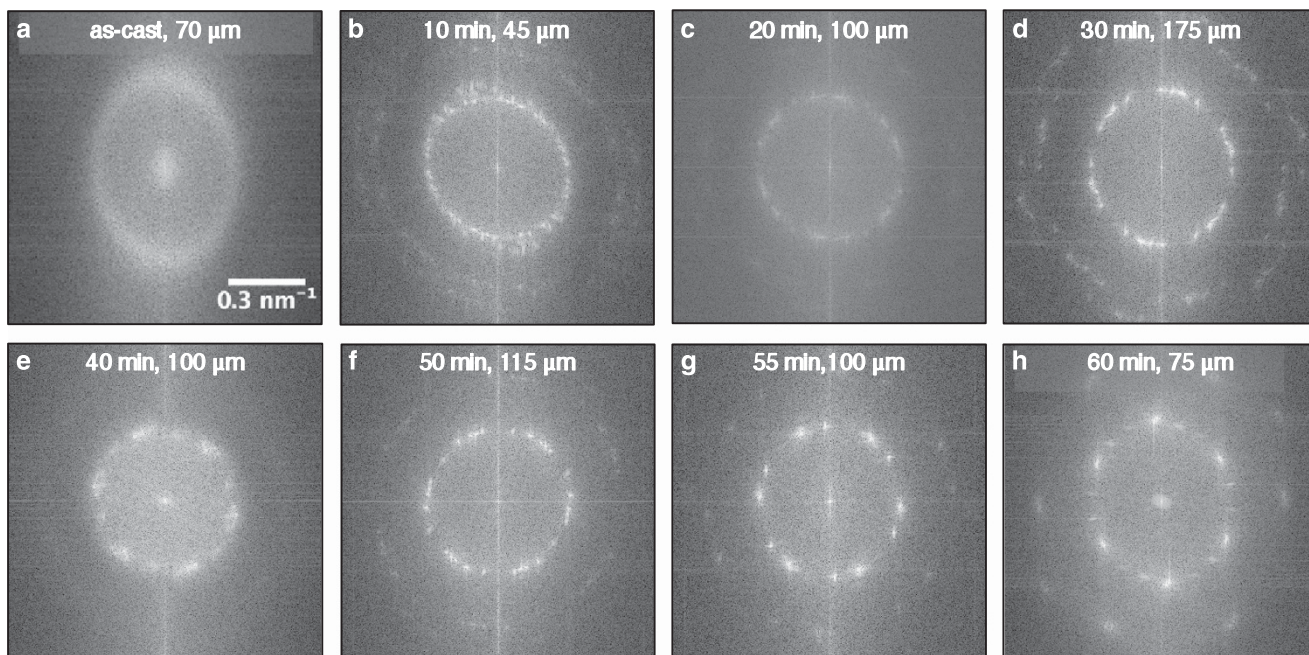
Figure 4 Fourier transform patterns obtained for the atomic force microscope images (phase images) shown in Figure 3. The scale bar in **a** is defined as $2\pi/d$, where d denotes the spacing in the real space image.
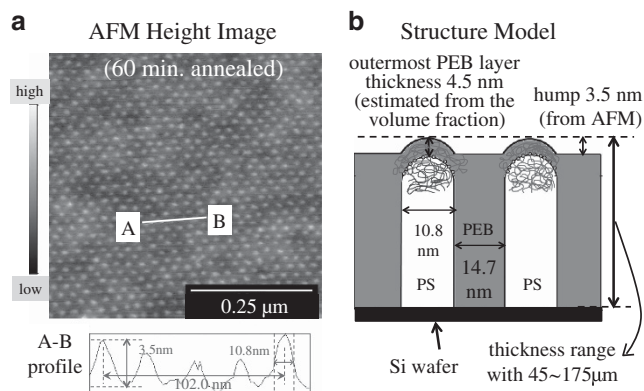

Figure 5 (**a**) Atomic force microscope (AFM) height image obtained for the specimen annealed at 210 °C for 60 min and (**b**) a plausible structure model based on the requirement of the lower surface free energy of poly(ethylene-*co*-butylene) (PEB), which should cover the free surface. A full color version of this figure is available at *Polymer Journal* online.

thickness was evaluated as 4.5 nm, which is slightly larger than the hump (3.5 nm) height determined from the AFM height image, as depicted in Figure 5b. This layer thickness is sufficiently thin for the phase image of the AFM to detect the PS cylinders existing beneath the surface. It has been revealed by a separate experiment[16] that phase imaging can detect the PS phase of other SEBS samples (with a PS volume fraction of 0.08) with thickness of the outermost PEB layer up to 10 nm. The existence of the outermost PEB layer was confirmed using X-ray photoelectron spectroscopy. Namely, it was confirmed that the characteristic peak for the PS component at 290.6 eV (C 1*s* $\pi \rightarrow \pi^{\star}$[27]) did not appear in the X-ray photoelectron spectroscopy spectrum measured by setting the take-out angle at 90° (normal to the specimen surface).[16] Note that the penetration depth of the X-ray was the deepest, but it was only 10 nm for this measurement

condition. As the penetration depth is identical to the thickness of the outermost PEB layer in the case of the separate experiment,[16] the signal from the PS phase cannot be detected. Therefore, it is reasonable to expect that the outermost PEB layer exists in the SEBS thin specimen with the PS volume fraction of 0.16 examined in the current study.

The finding that the PS cylinders were also oriented perpendicular to the film surface seemed to contradict common knowledge that cylinders tend to orient parallel to the surface in the proximity of the outermost surface of a block copolymer film. The reason for the perpendicular orientation at the surface may have been related to the formation mechanism of the PS cylinders through coalescence of the non-equilibrium PS spheres upon thermal annealing at 210 °C. As the directional coalescence of the spheres results in the perpendicular orientation, induction of the coalescence at the surface is considered to result in the perpendicular orientation of the cylinders at the specimen surface. It is noted here that the spheres are randomly arranged in Figure 3a. This means that a preferential orientation did not exist, although it was expected that the (110) planes of the body-centered cubic lattice would spontaneously orient parallel to the free surface. For the solution casting, the $\langle 111 \rangle$ direction is expected to be parallel to the migration path of the solvents in the solution state[22] because the spheres do not significantly block the solvent migration from the interior of the solution toward the free surface when the $\langle 111 \rangle$ direction is parallel to the migration path. Note here that the distance between neighboring $\langle 111 \rangle$ axes is the widest in the body-centered cubic packing case. It is further noted that the solvent migration path is vertical, and therefore, the $\langle 111 \rangle$ direction is eventually oriented perpendicular to the surface of the as-cast specimen. As the spheres are packed most densely in the $\langle 111 \rangle$ direction, which in turn indicates that the distance between the neighboring spheres in this direction is the closest, the spheres are more likely to coalesce with each other in this direction upon thermal annealing. This is a plausible mechanism of the formation of cylinders perpendicular to the surface of the specimen.

Even for the case when the coalescence is initiated in the interior of the specimen (distant from the surface), the growth front of the cylinders is considered to face the next nearest-neighboring sphere, which is in line with the normal direction of the film. Thus, chain reactions of coalescence can occur immediately, and this kind of chain reaction does not enable the PS spheres existing in the proximity of the surface to coalesce with each other to form cylinders oriented parallel to the surface. Although the AFM image obtained in the early stage of the thermal annealing suggests the existence of PS spheres, it was confirmed from the SAXS measurements, as shown below, that the formation of the cylinders was completed after 10 min. of annealing. As a matter of fact, we revealed that the formation of cylinders occurred as early as 102 s and was completed after 174 s during thermal annealing at 225 °C in our previous study from transmission electron microcopy and time-resolved SAXS measurements.[22] Therefore, 10 min of annealing at a slightly lower temperature (at 210 °C), as shown in Figure 3b, was acceptable for completing the cylinder formation. Nevertheless, it is possible to consider that the outermost morphology on the surface was not yet converted into a cylinder. Unfortunately, this possibility cannot be ruled out. Therefore, readers are asked to remember this possibility for the following discussions.

Figure 6 explains the fundamental steps of the image analysis method used in the current study to evaluate the grain area, which is the same method previously reported.[17] Staring with a, the AFM phase image for the specimen annealed at 210 °C for 60 min, we obtained b, which is the FT image of a. Actually, Figure 6b is the two-dimensional FT power spectra of the AFM image. The two-dimensional FT was performed according to the following formulation of the discrete FT using free ImageJ software.

$$F(q_k, q_l) = \sum_{m=1}^{M} \sum_{n=1}^{N} f(x_m, x_n) \exp(-iq_k x_m) \exp(-iq_l x_n) \quad (2)$$

where $F(q_k, q_l)$ is the FT of $f(x_m, x_n)$, which is the pixel value in the Cartesian coordinates of (x_m, x_n) for $1 \leqslant m \leqslant M$ and $1 \leqslant n \leqslant N$ in the AFM image with q_k and q_l defining the coordinates in the Fourier space for $1 \leqslant k \leqslant K$ and $1 \leqslant l \leqslant L$, given by

$$q_k = \frac{2\pi \, k}{\Delta x M} \quad (3)$$

$$q_l = \frac{2\pi \, l}{\Delta x N} \quad (4)$$

where Δx denotes the increment of x_m and x_n, namely, $\Delta x = x_{m+1} - x_m = x_{n+1} - x_n$. Then, the power spectra were calculated
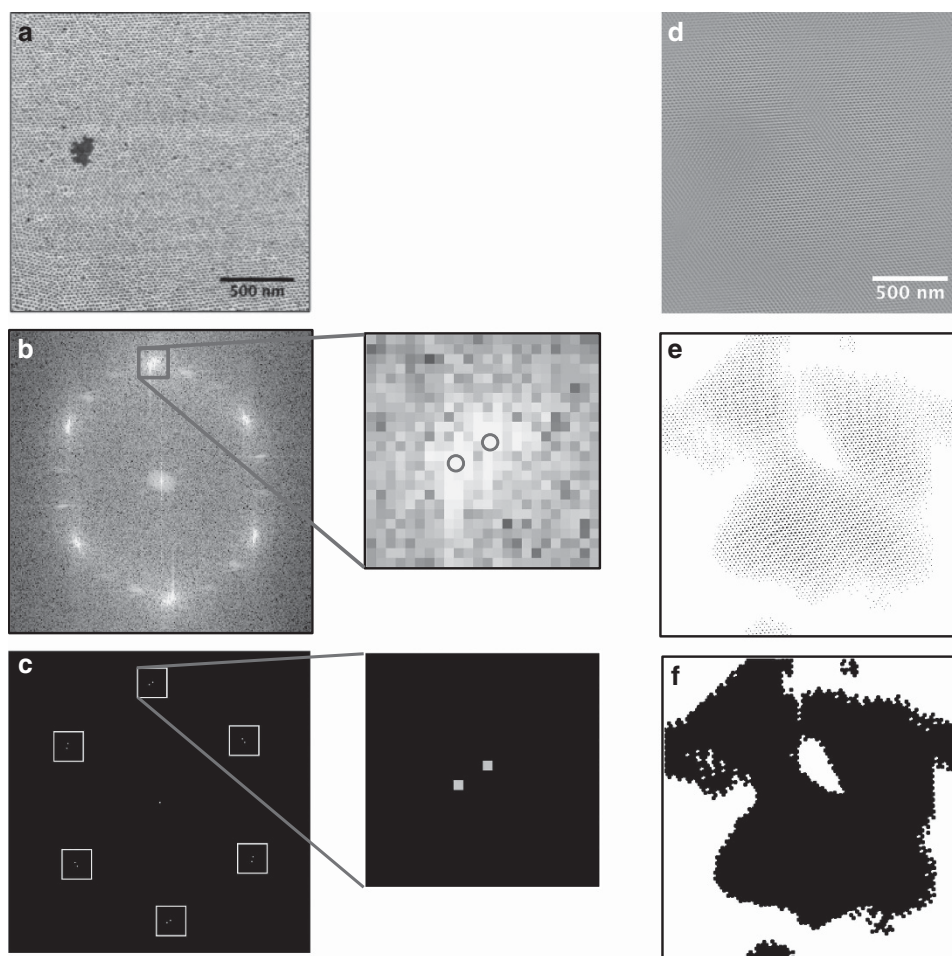

Figure 6 Images obtained from the image analyses to ultimately evaluate the grain area. (**a**) Atomic force microscope phase image for the specimen annealed at 210 °C for 60 min; (**b**) Fourier transform (FT) image of **a**; (**c**) masked image of **b**, in which the mask has 12 holes in total with a one-pixel-sized area; (**d**) inverse FT image; (**e**) binarized image of **d**; and (**f**) identification of a single grain (smeared in black). A full color version of this figure is available at *Polymer Journal* online.

using $F(q_k, q_l) \cdot F^*(q_k, q_l)$, where $F^*(q_k, q_l)$ denotes the complex conjugate of $F(q_k, q_l)$. In Figure 6b, a set of 6 bright spots is clearly shown. Close examination revealed that the pattern was composed of two sets of 6 spots. As one set of 6 spots corresponds to a single hexagonal region, the fact that two sets of 6 spots are shown in Figure 6b suggests the existence of two different hexagonal regions in the original AFM image. Therefore, we made a masked image with 12 holes (each hole has the diameter of one pixel), as shown in Figure 6c, to select these individual 12 spots for the purpose of the inverse FT. Note here that the inverse FT was conducted using $F(q_k, q_l)$ in ImageJ according to the following formulation:

$$f(x_m, x_n) = \frac{1}{K}\frac{1}{L}\sum_k \sum_l F(q_k, q_l)\exp(iq_k x_m)\exp(iq_l x_n) \quad (5)$$

Then, the inverse FT image highlighting the largest grain in the original AFM image (Figure 6a) was obtained as shown in Figure 6d in grayscale. As the grayscaled image is not clear, the image was binarized (Figure 6d) to obtain a clear image as shown in Figure 6e. By overlapping this image onto the original AFM image (Figure 6a), we could check the validity of the extraction of the grain from the original image. Namely, the process of extracting the grain was completed when the overlapped image (Figure 6e) was found to appropriately represent the original image. Otherwise, we returned to the position of the masking FT image (c) by selecting different sets of the bright spots, and followed the same procedure to obtain e. The appropriately selected single grain (the largest grain in the AFM image) was finally smeared in black, as shown in Figure 6f. Then, the area of the smeared region was evaluated using ImageJ, from which we calculated the diameter of the equivalent circle with the same value of the area. Hereafter, this diameter is referred to as the grain size.

On the basis of the image analysis results, the growth of the grain could be discussed as a function of the annealing time (annealed at 210 °C) in the course of the transformation from non-equilibrium PS spheres to equilibrium PS cylinders. To compare the grain growth in the interior of the specimen, it was quantitatively evaluated. For this purpose, 2d-SAXS measurements were conducted. The results of the 2d-SAXS measurements are shown in Figure 7 for the same specimens used for the AFM observations shown in Figure 3. The scale bar
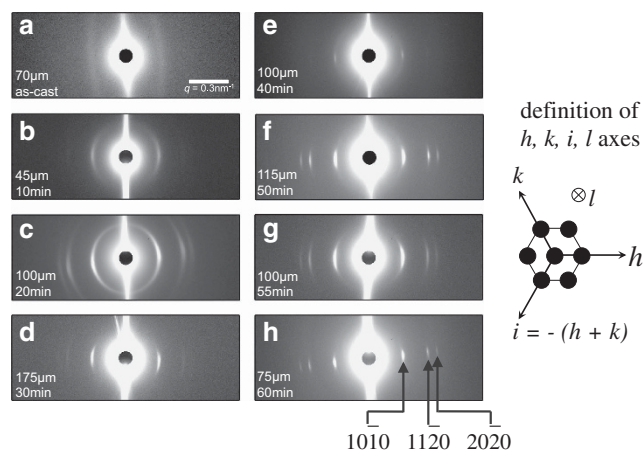
shown in panel a is 0.3 nm^{-1} of the magnitude of the scattering vector q. Note also that the direction of the film normal was vertical (in the meridional direction). Overall, for Figure 7c–h, reflection peaks from the hexagonal lattice of the cylinders can be observed, and they appear as arcs or spots that preferentially appear in the equatorial direction. This fact clearly indicates that the cylinders were preferentially oriented perpendicular to the film specimen inside. From the width of the arc, we evaluated the orientation factor by conducting the same method as reported before.[22] To evaluate the grain size, the width of the reflection peaks was determined from the one-dimensional SAXS (1d-SAXS) profiles. Figure 8 shows the corresponding 1d-SAXS profiles (semi-logarithmic plots of the scattering intensity $I(q)$ vs q) obtained from the 2d-SAXS patterns shown in Figure 7 after sector-averaging in the range $\phi \pm 2.5°$ of the azimuthal angle, where ϕ denotes the azimuthal angle for the direction of the reflection peak appearing. Here the positions of the first-order, second-order and third-order peaks are indicated by the broken vertical lines, which remained nearly constant during thermal annealing. After 20 min of annealing, the ratio of the peak positions could be relatively expressed as $1:\sqrt{3}:2$, suggesting reflections from the $\{10\bar{1}0\}$, $\{11\bar{2}0\}$ and $\{20\bar{2}0\}$ planes of the hexagonal lattice of the cylinders. According to the method by Hosemann,[28] the grain size was quantitatively evaluated using equation (6) from the peak width of the $\{10\bar{1}0\}$ and $\{20\bar{2}0\}$ reflections, respectively, as $m=1$ and 2, where m stands for the order of the reflection peaks.

$$(\Delta q)^2 = \left(\frac{2\pi}{D_G}\right)^2 + \left(\frac{2\pi^3 g^2}{\bar{d}}\right)^2 m^4 \quad (6)$$

where Δq is the integral width of the reflection peaks ($\Delta q = S/I_m$, where S and I_m denote, respectively, the peak area (integrated intensity) and the scattering intensity at the peak top). D_G is the average grain size, $\bar{d}$ is the average spacing of the planes and g stands for the lattice distortion factor, as defined by

$$g = \frac{\Delta d}{\bar{d}} \quad (7)$$

where Δd is the s.d. of the distribution of the spacing d. It should be noted here that the experimentally observed peak breadth contains an error due to the instrumental broadening. To correct for this effect, the following relationship should be used.

$$(\Delta q)^2 = (\Delta q')^2 - B^2 \quad (8)$$

where $\Delta q'$ denotes the observed peak width (integral width). Note here that $B^2 = 1.16 \times 10^{-4}$ (nm^{-2}) was estimated from the standard sample (chicken tendon collagen) according to the procedure provided in our previous paper.[18]

By conducting a computational peak decomposition of the 1d-SAXS profiles, the peak breadth, $\Delta q'$, was evaluated for the $\{10\bar{1}0\}$ and $\{20\bar{2}0\}$ reflections, respectively, as $m=1$ and 2. After the correction according to equation (8), the $(\Delta q)^2$ values were obtained. Figure 9 shows the plots of $(\Delta q)^2$ vs m^4 for the specimens annealed at 210 °C for 20–60 min. From the slope and intercept of the approximated line shown in Figure 9, values of the g-factor and D_G were estimated, respectively, and summarized in the plot against the annealing time in Figure 10. We now compare the results of the grain size in the vicinity of the surface and in the interior of the specimen. Before the discussion, it should be noted that the grain size plotted in Figure 10 denotes the extent of the grain in the direction perpendicular to the cylindrical axes, as schematically illustrated in Figure 1. The extent of the grains in the direction parallel to the cylindrical axes was not evaluated.
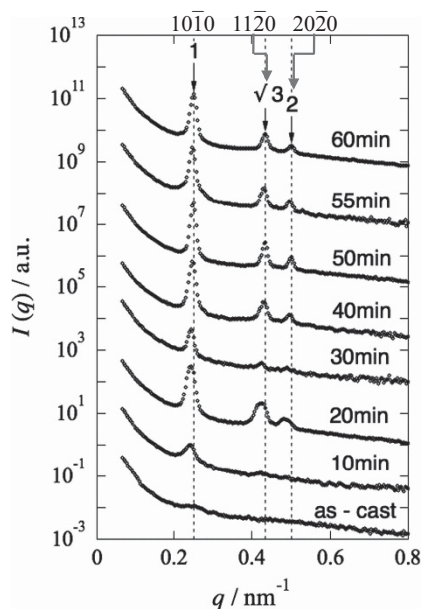

Figure 7 Two-dimensional small-angle X-ray scattering patterns (edge views) measured for the same specimens used for the atomic force microscope observation shown in Figure 3. The scale bar shown in **a** is 0.3 nm^{-1} of the magnitude of the scattering vector q. Note also that the direction of the film normal is vertical (in the meridional direction). A full color version of this figure is available at *Polymer Journal* online.

Figure 8 One-dimensional small-angle X-ray scattering profiles (semi-logarithmic plot of the scattering intensity $I(q)$ vs q) obtained from the two-dimensional small-angle X-ray scattering patterns shown in Figure 7 after sector-averaging in the range $\phi \pm 2.5°$ of the azimuthal angle, where ϕ denotes the azimuthal angle for the direction of the reflection peak appearing. A full color version of this figure is available at *Polymer Journal* online.
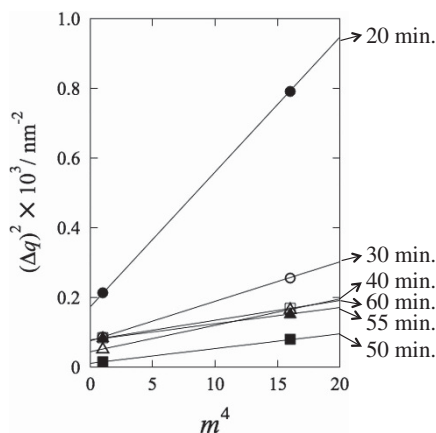

Figure 9 Plots of $(\Delta q)^2$ vs m^4 for the specimens annealed at 210 °C for 20–60 min. Here Δq is the integral width of the reflection peaks ($\Delta q = S/I_m$, where S and I_m denote, respectively, the peak area (integrated intensity) and the scattering intensity at the peak top) and m stands for the order of the reflection peaks ($m = 1, 2, 3, \ldots$ integer number).

From the comparison of the results, it was found that the grain was slightly larger (~53% larger) on the surface than in the interior of the specimen. However, this difference might have been due to the differences in the evaluation methods. Nevertheless, both results for the grain growth on the surface and in the interior of the specimen exhibited power-law behavior with the same exponent (~0.45) with <55 min of thermal annealing, during which the cylinders gradually oriented perpendicular to the film surface while simultaneously improving the hexagonal lattice regularity. Note that this power-law behavior has been reported before.[15,29] Nevertheless, the slope values
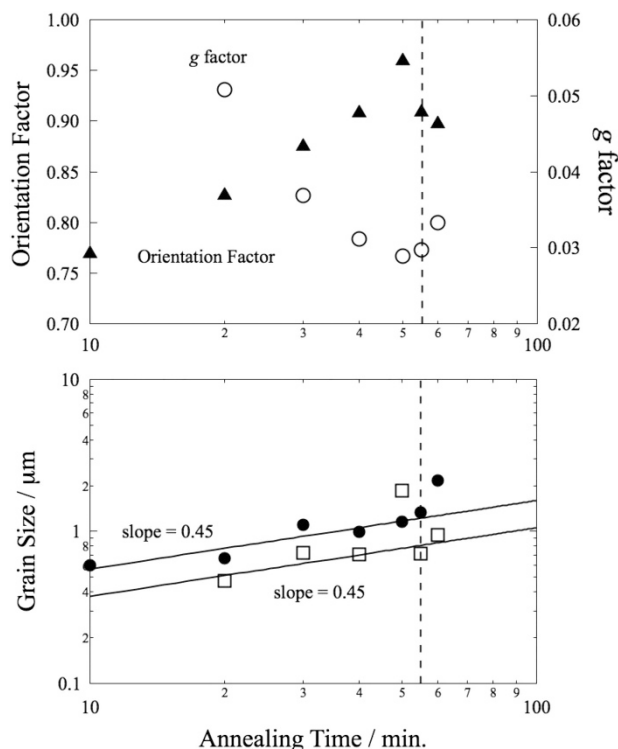

Figure 10 Plots of the orientation factor (closed triangles), the *g*-factor (open circles), the largest grain size evaluated from atomic force micrscopy (closed circles) and the average grain size evaluated from small-angle X-ray scattering (SAXS) (open squares) as a function of the annealing time (logarithmic scale). Note that the orientation factor was evaluated based on the two-dimensional SAXS results.

(power exponent values) were very much different from those reported by Hu et al.[29] They reported very small exponent values of ~0.1 for lamellae-forming PS-*block*-polyisoprene diblock copolymers. They investigated the grain growth with thermal annealing using transmission electron micrcopy, starting with small grains of lamellae in the as-cast specimens. Although the differences in the grain growth were acceptable for the different kinds of morphologies, our results showed significantly larger exponent values (0.45 in Figure 10). Regarding perpendicularly oriented cylinders in hexagonal lattices, computer simulations have been performed by Ohnogi and Shiwa.[30,31] Although the grain growth was not discussed in their original papers, it was possible to evaluate the grain growth exponent. They considered the phase-field-crystal model for the formation of microdomains and their ordering in block copolymers. The phase-field-crystal model is a typical example used for the simulation of conservative phase transitions. The basic equation is a type of the time-dependent Ginzburg–Landau equation. Ohnogi and Shiwa studied the formation of cylindrical microdomains from a disordered state. During the late stage, the grain growth of the hexagonal lattice was identified as being accompanied by the disappearance of the grain boundary and annihilation of defects in the ordered cylinders. It has been confirmed that inclusion of noise in a simulation affects the growth rate of grains. Hence, a term that generates noise was added to the model equation, and numerical calculations were performed. The power-law behavior was confirmed for the simulated results with an exponent of 0.15 without noise, and it increased up to 0.33 as the effect of noise increased. Compared with the values of the growth exponent, our result (0.45) is larger. It should be noted that the value of 0.33 for the

growth exponent is consistent with that for the Lifshitz–Slyozov process (evaporation-and-condensation process or Ostwald ripening).[32–34] This value indicates a random growth process. By contrast, the exponent of 1.0 is known as the Siggia's growth law,[35] in which hydrodynamic effects (in the presence of a pressure difference) accelerate the growth and elevate the value of the growth exponent. Therefore, our result is in between 0.33 and 1.0 and indicates that the growth is not merely governed by a random process but somewhat affected by hydrodynamic effects. This intermediate growth exponent value has been reported for the case of polymer blend phase separation processes (domain coarsening) under a temperature gradient, namely, in the presence of convective flow.[36] Thus, our result implies the existence of a pressure difference in the growing grains of the perpendicularly oriented cylinders both on the surface and in the interior of the specimen. The details of the pressure difference are unknown at present.

For thermal annealing longer than 55 min, an abrupt increase in the grain size is noticeable both on the surface and in the interior of the specimen. Therefore, it can be stated that the grains began to grow after the cylinders became perpendicularly oriented (the orientation factor reached a constant value, as shown in Figure 10). Note here that the orientation factor is defined as unity when the perpendicular orientation of the cylinders is perfect, while it is zero for random orientation. The behavior of the *g*-factor indicates that the hexagonal lattice regularity improved with annealing for < 55 min, while it did not change with more than 55 min of annealing. Note here that the lattice regularity defines the regularity of the hexagonal lattice existing in a grain in the interior of the specimen. That is, with < 55 min the cylinders gradually oriented perpendicular to the film specimen while simultaneously improving the hexagonal lattice regularity, and the grains also grew. Therefore, it can be concluded that the grains could not grow quickly during such structural changes (progressive perpendicular orientation of the cylinders and improvement in the hexagonal lattice regularity). After completing the orientation and improving the lattice regularity, the grains were finally able to grow quickly.

CONCLUSIONS

The surface morphologies of thin film specimens of SEBS triblock copolymers were characterized using AFM observations with perpendicularly oriented PS cylinders. We sought to determine whether the cylinder orientation was parallel or perpendicular to the surface of the film specimen and found that the cylinder orientation at the surface was also perpendicular. The result was attributed to the initiation mechanism of the directional coalescence of the non-equilibrium PS spheres. Furthermore, the grain size was successfully evaluated using AFM observations with an image analysis method using FT/inverse FT techniques for the grains in the proximity of the surface of the thin film specimens. The grain size in the interior of the specimen was also evaluated using SAXS measurements. After comparing the results, it was found that the grains were slightly larger (~53% larger) on the surface than in the interior of the sample. However, this discrepancy was attributed to the differences in the evaluation methods. Nevertheless, both results for the grain growth on the surface and in the interior of the sample exhibited power-law behavior with the same exponent (~0.45) with < 55 min of thermal annealing, in which the cylinders gradually oriented perpendicular to the film surface while simultaneously improving the hexagonal lattice regularity. By contrast, with more than 55 min of thermal annealing, an abrupt increase in the grain size was noticeable both on the surface and in the interior of the specimen. Therefore, it can be concluded

that the grains could not grow quickly during the structural changes in the interior of the specimen (progressive perpendicular orientation of the cylinders and improvement in the hexagonal lattice regularity). After completing the orientation and achieving lattice regularity, the grains were finally able to grow quickly.

1 Harrison, C., Adamson, D. H., Cheng, Z. D., Sebastian, J. M., Sethuraman, S., Huse, D. A., Register, R. A. & Chaikin, P. M. Mechanisms of ordering in striped patterns. *Science* **290**, 1558–1560 (2000).
2 Knoll, A., Horvat, A., Lyakhova, K. S., Krausch, G., Sevink, G. J. A., Zvelindovsky, A. V. & Magerle, R. Phase behavior in thin films of cylinder-forming block copolymers. *Phys. Rev. Lett.* **89**, 035501 (2002).
3 Knoll, A., Magerle, R. & Krausch, G. Phase behavior in thin films of cylinder-forming ABA block copolymers: experiments. *J. Chem. Phys.* **120**, 1105–1116 (2004).
4 Hexemer, A., Stein, G. E., Kramer, E. J. & Magonov, S. Block copolymer monolayer structure measured with scanning force microscopy Moiré patterns. *Macromolecules* **38**, 7083–7089 (2005).
5 Sakurai, S., Sakamoto, A., Itaya, A., Yamada, K., Mouri, E. & Matsuoka, H. Surface ordering of spherical microdomains of block copolymers. *Int. J. Appl. Chem.* **1**, 1–12 (2005).
6 Tomita, S., Shimizu, N., Igarashi, N., Takagi, H., Sasaki, S. & Sakurai, S. Coalescence of non-equilibrium spheres through thermal-annealing in an SEBS triblock copolymer film under a uniaxially stretched state. *Polym. J.* **49**, 519–526 (2017).
7 Horvat, A., Lyakhova, K. S., Sevink, G. J. A., Zvelindovsky, A. V. & Magerle, R. Phase behavior in thin films of cylinder-forming ABA block copolymers: mesoscale modeling. *J. Chem. Phys.* **120**, 1117–1126 (2004).
8 Okuda, H., Takeshita, K., Ochiai, S., Sakurai, S. & Kitajima, Y. Near-surface relaxation structure of annealed block copolymer film on Si substrates examined by grazing-incidence small-angle scattering utilizing soft X-rays. *J. Appl. Crystallogr.* **44**, 380–384 (2011).
9 Okuda, H., Takeshita, K., Ochiai, S., Kitajima, Y., Sakurai, S. & Ogawa, H. Contrast matching of an Si substrate with polymer films by anomalous dispersion at the Si K absorption edge. *J. Appl. Cryst.* **45**, 119–121 (2012).
10 Wernecke, J., Okuda, H., Ogawa, H., Siewert, F. & Krumrey, M. Depth-dependent structural change in PS-b-P2VP thin films induced by annealing. *Macromolecules* **47**, 5719–5727 (2014).
11 Saito, I., Miyazaki, T. & Yamamoto, K. Depth-resolved strucutre analysis of cylindrical microdomain in block copolymer thin film by grazing-incidnece small-angle X-ray scattering utilizing low-energy X-rays. *Macromolecules* **48**, 8190–8196 (2015).
12 Gunkel, X. G., Hexemer, A. & Russell, T. P. Controlling domain spacing and grain size in cylindrical block copolymer thin films by means of thermal and solvent vapor annealing. *Macromolecules* **49**, 3373–3381 (2016).
13 Yamamoto, K. in *X-ray Scattering* ed. Ares, A. E. Chapter 3, 61–88 (In Tech, Croatia, 2017).
14 Sakurai, S. Recent developments in polymer applications of synchrotron X-ray small-angle scattering (review article). *Polym. Int.* **66**, 237–249 (2017).
15 Honda, K., Sasaki, S. & Sakurai, S. [Spontaneous orientation of the body-centered-cubic lattice for spherical microdomains in a block copolymer thin film] (in Japanese). *Kobunshi Ronbunshu* **74**, 75–84 (2017).
16 Bayomi, R. A. H., Honda, K., Sasaki, S. & Sakurai, S. in preparation (2017).
17 Ohnogi, H., Isshiki, T., Sasaki, S. & Sakurai, S. Intriguing transmission electron microscopy images observed for perpendicularly oriented cylindrical microdomains of block copolymers. *Nanoscale* **6**, 10817–10823 (2014).
18 Ohnogi, H., Sasaki, S. & Sakurai, S. Evaluation of grain size by small-angle X-ray scattering for a block copolymer film in which cylindrical microdomains are perpendicularly oriented. *Macromol. Symp.* **366**, 35–41 (2016).
19 Igarashi, N., Watanabe, Y., Shinohara, Y., Inoko, Y., Matsuba, G., Okuda, H., Mori, T. & Ito, K. Upgrade of the small angle X-ray scattering beamlines at the Photon Factory. *J. Phys. Conf. Ser.* **272**, 012026 (2011).
20 Rasband, W. S. ImageJ, U. S. National Institutes of Health, Bethesda, Maryland, USA, 1997–2014. Available at http://imagej.nih.gov/ij/.

21 Sakurai, S. Progress in control of microdomain orientation in block copolymers efficiencies of various external fields. *Polymer* **49**, 2781–2796 (2008).

22 Sakurai, S., Bando, H., Yoshida, H., Fukuoka, R., Mouri, M., Yamamoto, K. & Okamoto, S. Spontaneous perpendicular orientation of cylindrical microdomains in a block copolymer thick film. *Macromolecules* **42**, 2115–2121 (2009).

23 Tomita, S., Lei, L., Urushihara, Y., Kuwamoto, S., Matsushita, T., Sakamoto, N., Sasaki, S. & Sakurai, S. Strain-induced deformation of glassy spherical microdomains in elastomeric triblock copolymer films: simultaneous measurements of a stress-strain curve with 2d-SAXS patterns. *Macromolecules* **50**, 677–686 (2017).

24 Tomita, S., Urakawa, H., Wataoka, I., Sasaki, S. & Sakurai, S. Complete and comprehensive orientation of cylindrical microdomains in a block copolymer sheet. *Polym. J.* **48**, 1123–1131 (2016).

25 Tomita, S., Shimizu, N., Igarashi, N., Takagi, H., Sasaki, S. & Sakurai, S. Time-resolved 2d-SAXS measurements to reveal mechanism of cylinder orientation upon sphere-to-cylinder transition under a planar flow in an SEBS triblock copolymer sheet. *Euro. Polym. J.* **93**, 382–389 (2017).

26 Tanaka, K., Takahara, A. & Kajiyama, T. Film thickness dependence of the surface structure of immiscible polystyrene/poly(methyl methacrylate) blends. *Macromolecules* **29**, 3232–3239 (1996).

27 Way, W. K., Rosencrance, S. W., Winograd, N. & Shirley, D. A. Polystyrene by XPS. *Surf. Sci. Spectra* **2**, 67–70 (1993).

28 Hosemann, R., Lemm, K. & Wilke, W. The pracrystal as a model for liquid crystals. *Mol. Cryst.* **1**, 333–362 (1967).

29 Hu, X., Zhu, Y., Gido, S. P., Russell, T. P., Iatrou, H., Hadjichristidis, N., Abuzaina, F. M. & Garetz, B. A. The effect of molecular architecture on the grain growth kinetics of AnBn star block copolymers. *Faraday Discuss.* **128**, 103–112 (2005).

30 Ohnogi, H. & Shiwa, Y. Nucleation, growth, and coarsening of crystalline domains in order-order transitions between lamellar and hexagonal phases. *Phys. Rev. E* **84**, 011611 (2011).

31 Ohnogi, H. & Shiwa, Y. Effect of noise on ordering of hexagonal grains in a phase-field-crystal model. *Phys. Rev. E* **84**, 051603 (2011).

32 Lifshitz, I. M. & Slyozov, V. V. The kinetics of precipitation from supersaturated solid solutions. *J. Phys. Chem. Solids.* **19**, 35–50 (1961).

33 Gunton, J. D., San Miguel, M., Sahni, P. S. in *Phase Transition and Critical Phenomena* Vol. 8: eds Dom, C. & Letowitz, J. L. 267 (Academic, London, 1983).

34 Kawasaki, K. & Ohta, T. Kinetics of fluctuations for systems undergoing phase transitions—interfacial approach. *Physica* **118A**, 175–190 (1983).

35 Siggia, E. D. Late stage of spinodal decomposition in binary mixtures. *Phys. Rev. A* **20**, 595–600 (1979).

36 Nambu, T., Yamauchi, Y., Kushiro, T. & Sakurai, S. Micro-convection, dissipative structure and pattern formation in polymer blend solutions under temperature gradients. *Faraday Discuss.* **128**, 285–298 (2005).